Smart Structures and Systems, *Vol. 34, No. 5 (2024) 335-351*
https://doi.org/10.12989/sss.2024.34.5.335

Effect of mesoscale randomness of various aggregates on stress wave propagation for debond detection of RCFSTs

Jiang Wang [1a], Bin Xu*[1,2], Qian Liu [1], Ruiqi Guan [1,2], Xiaoguang Ma [3] and Genda Chen [4,5]

[1] *College of Civil Engineering, Huaqiao University, Xiamen 361021, China*
[2] *Key Laboratory for Intelligent Infrastructures and Monitoring of Fujian Province (Huaqiao University), Xiamen 361021, China*
[3] *Foshan Graduate School, Northeastern University, Foshan 528311, China*
[4] *Department of Civil, Architectural and Environmental Engineering, Missouri University of Science and Technology, Rolla, MO 65401, USA*
[5] *INSPIRE University Transportation Center, College of Engineering and Computing, Missouri University of Science and Technology, Rolla, MO 65401, USA*

(*Received June 15, 2023, Revised September 14, 2024, Accepted December 22, 2024*)

Abstract. Concrete core in concrete-filled steel tubes (CFSTs) is heterogeneous at mesoscale and the heterogeneity affects stress wave propagation within CFSTs. Coupling homogenization finite element models (CHFEMs) corresponding to traditional coupling mesoscale finite element models (CMFEMs) of rectangular CFSTs (RCFSTs) with randomly distributed elliptical and polygonal aggregates are established. The influences of concrete core heterogeneity and an interface debond defect on stress wave field and the responses of piezoelectric-lead-zirconate-titanate (PZT) sensors at different measurement distances are distinguished using homogenization finite element models (HFEMs) and the CHFEMs, respectively. A comparative test on thirty RCFST cross sections with and without an interface debond defect is performed to quantitatively evaluate the effect of concrete core heterogeneity on the responses of PZT sensors at different measurement distances and to distinguish it with that of the designed interface debond defect. Both mesoscale homogenization numerical simulation and test results show that the heterogeneity and mesoscale randomness of concrete core locally affect the response of PZT sensors that are close to the PZT actuator mounted on the surface of the steel tube of the CFSTs at certain levels. The influence of the interface debond defect on the stress wave fields within the cross sections of RCFSTs and the response of PZT sensors with measurement distances over 160 mm is dominant. The findings further illustrate the rationality of the interface debond defect detection method using stress wave measurement of PZT sensors with a suitable measurement distance for RCFSTs even concrete core in RCFSTs in practice is a heterogenous material with randomly distributed aggregates of different shapes at mesoscale.

Keywords: acoustic; concrete/reinforced concrete; dynamic analysis; experiment; finite element method; nondestructive evaluation; numerical material modelling; piezoelectric sensors and actuators; time domain

1. Introduction

Complex concrete-filled steel tubes (CFSTs) have been extensively used as vertical or axial load-carrying components in high-rise buildings and long-span bridges (Feng *et al*. 2017). CFSTs have advanced mechanical performance due to the beneficial interaction between concrete core and steel tube (Gwon *et al*. 2020). However, owing to the unavoidable shrinkage and uneven temperature distribution of bulk concrete core during the process of curing and hardening, interface debond defects between concrete core and steel tube may occur (Li *et al*. 2016). The interface debond defect eventually reduces the confinement effect of steel tube on concrete core and results in a weakened load-carrying capacity, stiffness and ductility of CFST members (Liao *et al*. 2019, Liu *et al*. 2020). Therefore, it has been a common concern to develop reliable interface debond defect detection technology for CFSTs (Yan *et al*. 2018, Chen *et al*. 2021).

Due to the electromagnetic shielding (EMS) function of steel tubes, the complexity of inner structure and possible irregular cross-section of CFSTs in practice, it is very hard to detect the interface debond defects with most of traditional non-destructive testing (NDT) methods (Beena *et al*. 2017, Song *et al*. 2019). Aiming at the interface debond detection for CFSTs, Xu *et al*. firstly proposed a stress wave measurement based approach using embedded piezoelectric-lead-zirconate-titanate (PZT) sensors and experimentally validated the feasibility of the proposed approach for rectangular CFST (RCFST) specimens with artificially mimicked interface debond defects (Xu *et al*. 2013a, b). Besides, in order to investigate the mechanism of the active interface debond defect detection method for CFST members with PZT-based technology, as the pioneer researchers, Xu *et al*. have conducted comprehensive numerical simulations on the stress wave fields and the response of PZT sensors within or on the outer surface of rectangular and circular CFSTs under different excitation signals with finite element method (FEM), where the coupling effect between steel tube and concrete core and the

*Corresponding author, Ph.D., Professor,
E-mail: binxu@hqu.edu.cn
[a] Ph.D. Candidate, E-mail: Jiangwang@hqu.edu.cn

ISSN: 1738-1584 (Print), 1738-1991 (Online)

direct and inverse piezoelectric effects of PZT sensors and actuators are considered (Xu *et al*. 2017a, b, c). Xu *et al*. and Luan *et al*. proposed spectral element method (SEM) using absorbing layers to investigate the mechanism for interface debonding detection for CFST cross sections (Xu *et al*. 2020, Luan *et al*. 2021). Xu *et al*. experimentally investigated the feasibility of active interface debonding detection for RCFST with surface wave measurement (Xu *et al*. 2019). The stress wave measurement based defect detection approach was employed to detect grout defects for grouted splice sleeve connectors (Xu *et al*. 2021). Considering the coupling effect between PZT patches and CFST members, an electro-mechanical impedance (EMI) based interface debonding detection approach was proposed and employed to detect and localize the debonding in CFST specimens (Liu *et al*. 2024a, b). However, in most of the current structural analysis and stress wave propagation simulation studies, the concrete core is generally regarded as a homogeneous material at macroscale and the randomness and heterogeneity of concrete core in CFSTs at mesoscale are not considered (Mei *et al*. 2023, Abbas *et al*. 2023). When concrete is assumed as a homogeneous material, the simulation analysis on the macroscale mechanical behavior of concrete materials and structures cannot exactly reflect the influence of the heterogeneity and randomness of concrete on the overall mechanical behavior and local failure procedure (Dong *et al*. 2021, Wang *et al*. 2022c, Cai and Deng 2023).

In fact, concrete core in CFSTs is a typical composite material including multi-phase media such as mortar matrix, aggregates and the interface transition zone (ITZ) between mortar and aggregates matrix, etc. (Chen *et al*. 2018, Geng *et al*. 2022). It is critical to study the mechanical mechanism of concrete as a classic heterogeneous composite material at macroscale, mesoscale and microscale scales (Fu *et al*. 2019, Hu *et al*. 2022). Mesoscale modeling methods for concrete are crucial for effectively forecasting the mechanical properties of plain concrete, reinforced concrete (RC), steel-concrete composite structures such as CFST structures at mesoscale (Shen *et al*. 2019, Gu *et al*. 2019, Elias and Cusatis 2022, Jin *et al*. 2023).

Therefore, further investigation on the feasibility of the stress wave measurement-based interface debond defect detection approach for CFST members is desired, where the concrete core is considered as a typical heterogeneous composite material with randomly distributed aggregates with different shapes at mesoscale. In order to address the concern about the influence of mesoscale structure of concrete core on the stress wave propagation and the response of the PZT sensors within CFSTs, with the help of mesoscale concrete modelling approach, Xu *et al*. (2018) firstly established mesoscale RCFST models considering the random distribution of circular aggregates in concrete core and carried out multi-physics and mesoscale simulation on the stress wave fields and the responses of embedded PZT sensors in RCFST members without and with interface debond defects. By comparing the influence of the heterogeneity and randomness of mesoscale concrete and the interface debond defect on stress wave measurements of a PZT sensor at a constant measurement distance, the dominance of the influence of interface debond defect is illustrated. The limitation of the above study is that only circular aggregates are considered in the multi-physics and mesoscale simulation analysis.

Besides, considering the convenience of measuring surface wave along the steel tube of RCFST members, Chen *et al*. (2019) proposed a multichannel analysis of surface waves (MASW) method for detecting the interface debond defect in RCFST members and carried out mesoscale stress wave propagation to illustrate its mechanism. Wang *et al*. (2022a) established a coupling multi-physics CFST substructure model composed of circular aggregates and mortars with absorbing boundaries to explore the influence of the mesoscale concrete core on PZT sensors response. One of the disadvantages of the above mesoscale numerical models is their low computational efficiency and high computation resource needs coming with fine finite elements and short integration time steps required for computation accuracy and convergence requirements. Thus, further efforts are required to develop computational efficiency approaches for mesoscale simulation on stress wave fields and PZT sensor responses to investigate the influence of the heterogeneity of concrete core in the form of randomly distributed aggregates of different shapes and distinguish it with that of interface debond defect.

In recent years, to enhance the mesoscale numerical simulation efficiency for concrete materials and structures, a homogenization approach using representative volume elements (RVEs) based on composite materials theory has been proposed (Jin 2014, Rezakhani *et al*. 2017, Baxter *et al*. 2020, Abbès *et al*. 2020, Arkadiusz *et al*. 2021). The accuracy and computational efficiency of the proposed mesoscale homogenization approach with RVEs of different dimensions are verified and the influence of the heterogeneity and randomness of mesoscale concrete on the macroscale mechanical properties of concrete materials and structures are investigated. Based on the work by Xu *et al*. (2018), Wang *et al*. (2022b) proposed a mesoscale homogenization method using RAEs for two-dimensional (2D) RCFSTs with randomly distributed elliptical, polygonal and circular aggregates to numerically explore the influence of the mesoscale concrete core and interface debond defects on the stress wave field and the response of an embedded PZT sensor with a constant measurement distance of 80 mm in RCFSTs. In the study by Wang *et al*. (2022b), the effect of the dimension of RAEs on stress wave fields and PZT sensor measurement simulation results was not investigated and the difference of the influence of mesoscale heterogeneity of concrete core on PZT sensor measurements at different measurement distances was not numerically or experimentally addressed. Therefore, in order to address these two issues, Wang *et al*. (2023) numerically studied the stress wave fields for RCFST members using RAEs with different dimensions and then investigated the difference in PZT sensor responses at different measurement distances using mesoscale homogenization approach. In the study by Wang *et al*. (2023), only circular aggregates were considered in the mesoscale homogernization models, and no experimental verification on the influence of concrete core heterogeneity

and randomness on PZT sensor measurements at different measurement distances was performed. Further numerical and experimental investigations on the difference in the influence of the heterogeneity and randomness of concrete core in the form of different aggregate shapes on PZT sensors at different measurement distances are desired.

In this paper, different from the previous studies (Wang *et al*. 2022b, 2023), mesoscale simulation on stress wave fields and PZT sensors at different measurement distances of RCFST cross-sections with randomly distributed elliptical and polygonal aggregates is carried out to further distinguish the influence of the heterogeneity and randomness of concrete core in the form of the randomly distributed aggregates with different shapes with them of interface debond defects on the stress wave fields and the response of PZT sensors at different measurement distance for RCFSTs. Homogenization finite element models (HFEMs) corresponding to the mesoscale finite element models (MFEMs) of RCFSTs with randomly distributed elliptical and polygonal aggregates are established, respectively, to simulate the stress wave fields of the models. Coupling homogenization finite element models (CHFEMs) corresponding to the coupling mesoscale finite element models (CMFEMs) for RCFSTs with randomly distributed aggregates with different shapes are employed to simulate the responses of PZT sensors at different measurement distances. Moreover, the amplitude and the wavelet packet energy of PZT sensor measurements at different measurement distances under either sinusoidal or modulated excitation signals in CHFEMs with and without an interface debond defect are compared. The difference between the effect of the heterogeneity of concrete core in the form of randomly distributed elliptical and polygonal aggregates on different PZT sensor responses and that of the interface debond defect is also illustrated. Finally, experimental validation on thirty plane RCFST cross section specimens with different PZT sensor measurement distances under both sinusoidal and modulated excitation signals are carried out. Both numerical simulation and experimental studies show that the heterogeneity of concrete core in the form of the randomly distributed aggregates with different shapes in different RCFSTs induces limited variation in the response of PZT sensors close to the PZT actuator and has no obvious influence on the response of the PZT sensor far from the PZT actuator. Instead, the interface debond defect results in obvious variation in each PZT sensor measurement, compared with the heterogeneity of concrete core and the diversity of randomly distributed aggregate shape. The experimental validation is consistent with those from the numerical studies.

Table 1 Material parameters

Material	Young's modulus (GPa)	Poisson's ratio	Density (kg/m^3)
Aggregates	55.5	0.16	2700
Mortar	26	0.22	2100
Steel	207	0.28	7800
PZT	74	0.36	7600

Both the mesoscale and multi-physics simulation results and the experimental measurements testify the rationality of the interface debond detection approach for RCFSTs using stress wave measurements from PZT sensors at suitable measurement distances where the concrete core is a heterogeneous and random material in practice.

2. Modelling approach for CHFEMs with randomly distributed aggregates with different shapes

Concrete heterogeneity is mainly caused by various factors such as aggregate shape, distribution, and uneven pore structure. In this study, the concrete heterogeneity is represented by the randomly distributed aggregates with different shapes but the possible pores are not considered. To investigate the influence of the heterogeneity of concrete core and the diversity of the randomly distributed aggregate shapes on the stress wave fields and the response of PZT sensors at different measurement distances, a total of nine mesoscale RCFST models with randomly distributed circular, elliptical and polygonal aggregates are firstly established using the random aggregate method (RAM) (Xu *et al*. 2018, Wang *et al*. 2022b). In the previous study by Wang *et al*. (2022b), the effect of the concrete heterogeneity in the form of randomly distributed circular aggregates on an embedded PZT sensor at a measurement distance of 80 mm only is numerically investigated. In each RCFST specimen in this study, five PZT sensors with different measurement distances of 80 mm, 160 mm, 240 mm, 320 mm and 410 mm, are considered, respectively. The aggregate content in each RCFST specimen is identical and takes the value of 50%.

The size and quantity of randomly distributed circular, elliptical and polygonal aggregates in each CHFEM are specified using the Fuller gradation curve (Wang *et al*. 2022b). In this study, the characteristic diameters of the aggregates are set to 60 mm, 30 mm and 15 mm, which are employed to represent the typical dimension of bigstones (40–80 mm), middlestones (20–40 mm) and small stones (5–20 mm), respectively, in practice.

The dimensions of each RCFST and the material parameters of the mortar, aggregates, steel tube and PZT are

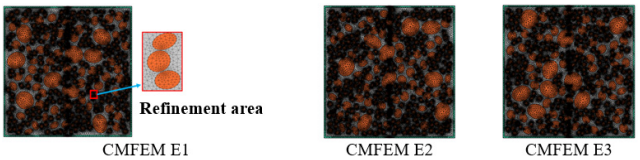

(a) Elliptical aggregate models

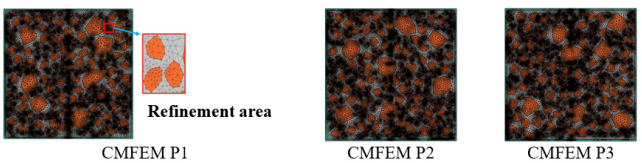

(b) Polygonal aggregate models

Fig. 1 Mesoscale RCFSTs considering randomly distributed aggregate with different shapes

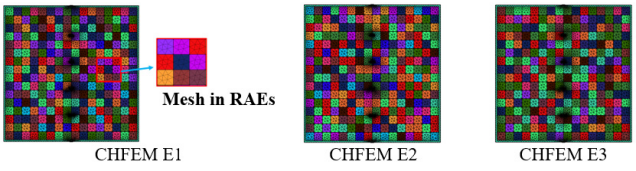

(a) Elliptical aggregate

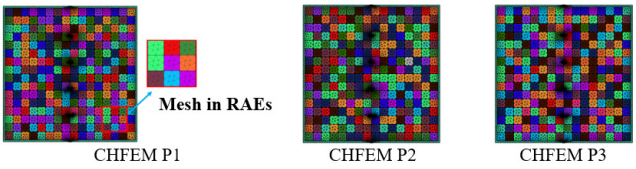

(b) Polygonal aggregate

Fig. 2 CHFEMs corresponding to the mesoscale RCFSTs shown in Fig. 1

listed in Table 1 (Wang *et al*. 2022b) Since the CHFEMS with circular aggregates have been discussed in previous study (Wang *et al*. 2023), six CHFEMs corresponding to the six CMFEMs with randomly distributed elliptical and polygonal aggregates are investigated in this paper. The mesoscale models and the corresponding finite element meshes of the six established CMFEMs named CMFEM E1-E3 and P1-P3 are shown in Fig. 1 and the corresponding CHFEMs are named CHFEMs E1-E3 and P1-P3 for simplicity.

The dimension of the finite elements for the six CMFEMs as shown in Fig. 1 should not exceed one-fifth of the wavelength of stress wave in the medium to avoid computation divergence (Xu *et al*. 2017a, b). Since concrete cores are heterogeneous at mesoscale, the meshing of each CMFEM has refinement regions as shown in Fig. 1. The numerical simulation on stress wave fields and the response of PZT sensors is computationally inefficient because of large number of elements and degree of freedoms (DOFs) in each mesoscale model. Therefore, to enhance computation efficiency for stress wave fields and the responses of PZT sensors of CMFEMs with either randomly distributed elliptical or polygonal aggregates, the corresponding CHFEMs are established and employed to explore the influence of interface debond defect, the heterogeneity of mesoscale concrete core and the shape diversity of randomly distributed aggregates on the stress wave fields and the responses of PZT sensors at different measurement distances under different excitation signals.

Fig. 2 shows the established CHFEMs corresponding to the six mesoscale CMFEMs for RCFSTs exhibited in Fig. 1 using the equivalent homogenization method (Jin 2014, Wang *et al*. 2022b), where the material properties of each RAE is homogenous. The material properties of each RAE are different because of various area fractions of mortar and aggregate in each RAE. Due to space limitations, the material properties of each RAE are not listed here. The dimension of each RAE used here is 25 mm by 25 mm based on the previous investigation results on the size effect of RAE on stress wave fields (Wang *et al*. 2023). As shown in Figs. 1 and 2, the number of finite elements of each CHFEM is far less than that of the corresponding CMFEM. Besides, the comparison of the element numbers, DOFs between the healthy CMFEMs and their corresponding CHFEMs is shown in Table 2, where the information of CMFEMs 1-3 with circular aggregate and the corresponding CHFEMs 1-3 is from the previous research of Wang *et al*. (2023). It is easy to understand that less simulation cost with CHFEMs is required when compared with that of the corresponding CMFEMs.

To further distinguish the influence of the hetergenerity and randomness of mesoscale concrete core and an interface debond defect on both stress wave fields and the output signals measured by PZT sensors at different measurement distances, additional six CHFEMs with an interface debond defect and identical mesoscale concrete core to the above CHFEMs are investigated. The six CHFEMs with an interface debond defect are called CHFEMs E1D-E3D and P1D-P3D, respectively. The interface debond defect has a length of 50 mm along the steel tube and a thickness of 4 mm.

The setting of the mechanical boundary of the coupling models and the electrical boundary for PZT patches is identical to that described in the study by Chen *et al*. (2019). In the stress wave fields simulation, the coupling effect between the PZT actuator or sensor and the RCFST member is not considered and the homogenization finite element models (HFEMs) corresponding to each CHFEM are employed for similarity. The stress wave fields in all HFEMs are determined by directly applying an excitation force on the location of PZT actuator. When simulating the response of each PZT sensor under sinusoidal and modulated signals, the inverse and direct piezoelectric effects of both PZT actuator and sensor and the multi-physics coupling effect between PZT patches and the RCFST are considered (Xu *et al*. 2017c, Chen *et al*. 2019). The control equations for stress wave propagation simulation of both CMFEMs and their corresponding CHFEMs have been described in literature and are shown as follows (Xu *et al*. 2018).

$$\begin{bmatrix}[M] & [0]\\ [0] & [0]\end{bmatrix}\begin{Bmatrix}\{\ddot{\mu}\}\\ \{\ddot{V}\}\end{Bmatrix}+\begin{bmatrix}[C] & [0]\\ [0] & [0]\end{bmatrix}\begin{Bmatrix}\{\dot{\mu}\}\\ \{\dot{V}\}\end{Bmatrix}+\begin{bmatrix}[K] & [K^Z]\\ [K^Z]^T & [K^d]\end{bmatrix}\begin{Bmatrix}\{\mu\}\\ \{V\}\end{Bmatrix}=\begin{Bmatrix}\{F\}\\ \{Q\}\end{Bmatrix} \tag{1}$$

where $[M]$ represents the mass matrix, $[K]$ is the matrix of stiffness, $[C]$ denotes the damping matrix, $\{\mu\}$ stands

Table 2 Comparison of calculating amount between CMFEMs and CHFEMs

	CHFEMs	CMFEM C1	CMFEM C2	CMFEM C3	CMFEM E1	CMFEM E2	CMFEM E3	CMFEM P1	CMFEM P2	CMFEM P3
Element number	25,561	68,788	68,706	68,413	73,018	73,716	76,346	75,650	74,318	74,151
DOFs	102,866	271,286	275,462	274,288	273,730	290,386	278,386	280,506	306,506	285,706

for the displacement vector of the RCFST member $[K^d]$ represents the matrix of dielectric and $[K^Z]$ is the electromechanical coupling matrix, $\{Q\}$ and $\{V\}$ are the quantity of electric charge and the electric potential on electrode surface, respectively, and $\{F\}$ represents the load vector.

The applied pulse force signal for stress wave fields simulation and the sinusoidal and modulated excitation signals for PZT sensor measurement simulation are identical to them in the previous study (Wang *et al*. 2022b). The modulated excitation signal for PZT sensor measurement simulation is listed below.

$$V_t = V_0 \sin(2\pi f t) \sin\left(\frac{2\pi f t}{10}\right)^2 \quad (2)$$

where V_t is the input voltage signal and V_0 represents the amplitude of input signal whose value is 10 V. f stands for frequency 20 kHz of the input signal. t is the time instant and takes the value of 2e - 7s.

3. Influence of mesoscale heterogeneity and randomness of concrete core with randomly distributed aggregates of different shapes and that of the interface debond on stress wave fields of HFEMs

In this section, mesoscale numerical simulation on stress wave fields of the six healthy HFEMs and the six HFEMs with an interface debond defect under pulse force with a frequency of 100 kHz is carried out, as a numerical investigation into the influence of the heterogeneity and randomness of mesoscale concrete core with randomly distributed aggregates of different shapes on stress wave fields and the comparison with that of interface debond defect.

3.1 Stress wave fields of HFEMs with randomly distributed elliptical aggregates

The stress wave fields of the three HFEMs E1-E3 with randomly distributed elliptical aggregates at three different time instants are displayed in Fig. 3, along with that of three corresponding HFEMs E1D-E3D with an interface debond defect. Comparing the stress wave fields of the three healthy HFEMs with different concrete core mesoscale structures at each identical time instant, it can be found that the randomly distributed elliptical aggregates in RCFSTs have no obvious influence on the stress wave fields. Similarly, comparing the stress wave fields of the three HFEMs E1D-E3D with an identical debond defect considering different concrete core mesoscale structures at each identical time instant as exhibited in Fig. 3, the consistency of stress wave fields of the three HFEMs E1D-E3D is also observed. Compared with the stress wave fields of the HFEMs without an interface debond defect with those of the HFEMs with an identical interface debond defect, it can be observed that the stress wave fields of the corresponding HFEMs with an identical interface debond defect show an obvious time delay and attenuation due to the existence of interface debond defect, indicating that it is the interface debond defect that affects the stress wave fields of RCFST members, instead of the randomly distributed elliptical aggregates in concrete core.

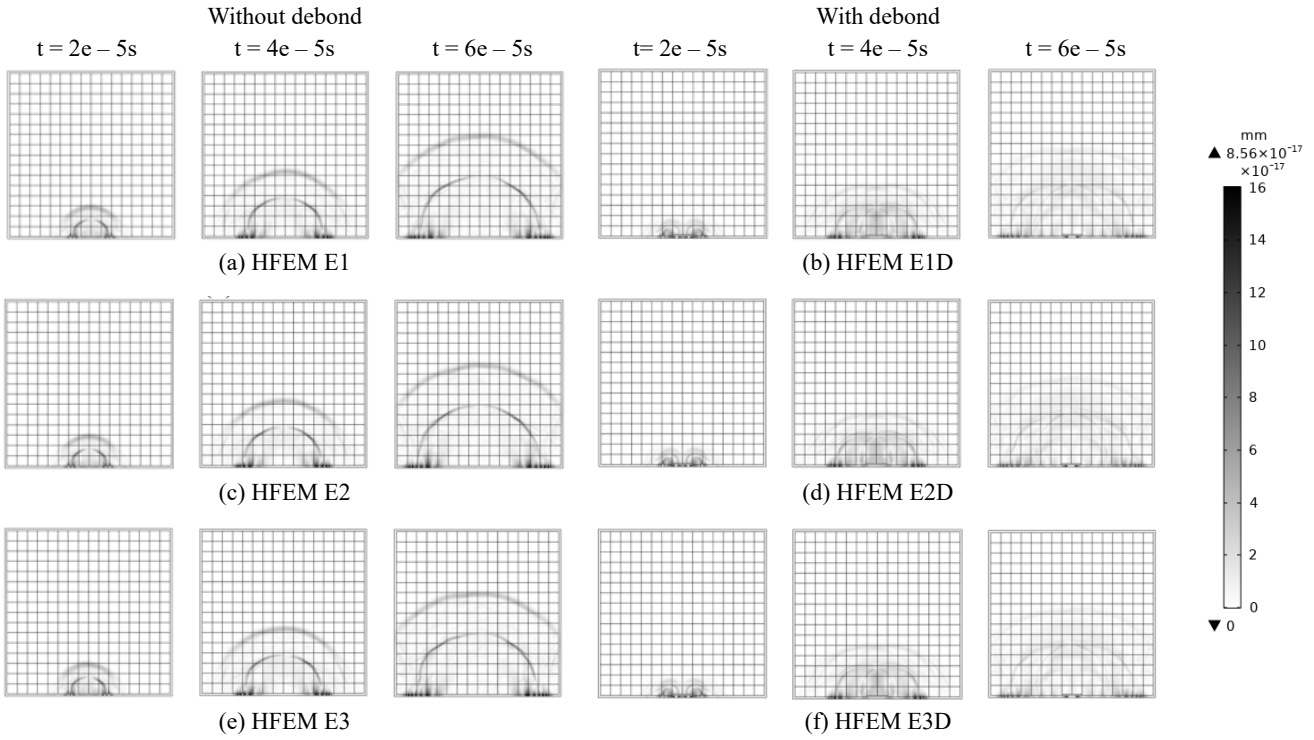

Fig. 3 Stress wave fields of HFEMs with and without an interface debond defect at different time instants

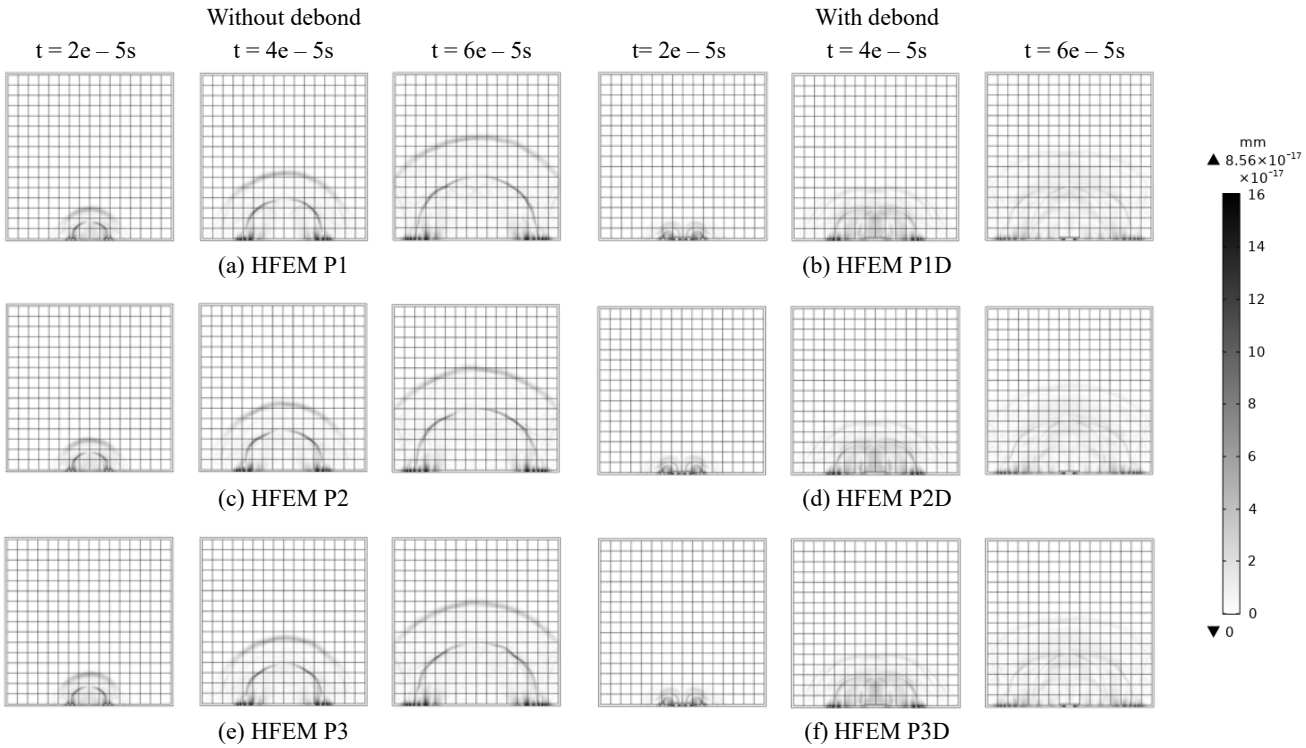

Fig. 4 Stress wave fields of HFEMs with and without an interface debond defect at different time instants

3.2 Stress wave fields of HFEMs with randomly distributed polygonal aggregates

The stress wave fields of the three HFEMs P1-P3 with randomly distributed polygonal aggregates and those HFEMs P1D-P3D with an identical interface debond defect are given in Fig. 4. The consistency of the stress wave fields of the three healthy HFEMs P1-P3 at each identical time instant can be found. Moreover, the consistency of the stress wave fields of the three HFEMs P1D-P3D with an identical interface debond defect also exists. Moreover, the influence of the interface debond defect on the stress wave fields in the form of travelling time delay and attenuation can be found clearly.

From the stress wave field simulation results shown in Figs. 3-4, it is clear that the interface debond defect is the dominant factor affecting the stress wave fields of RCFST members instead of the heterogeneity and randomness of the mesoscale concrete core and the shape diversity of randomly distributed aggregates.

To further distinguish the influence of the heterogeneity of the mesoscale concrete core and the shape diversity of randomly distributed aggregates on the responses of PZT sensors at different measured distances, the PZT sensor responses of the six healthy CHFEMs and the corresponding six CHFEMs with an identical interface debond defect under both sinusoidal and modulated excitation signals are investigated in the following section.

4. Influence of mesoscale structure and interface debond on PZT sensor rsponses at different measurement distances

This section simulates the PZT sensor responses at different measurements of the six healthy CHFEMs and the corresponding six CHFEMs with an identical interface debond defect under both sinusoidal and modulated excitation signals. The frequency of both the one-cycle sinusoidal signal and the five-cycle modulated signal is set to be 20 kHz. The amplitude of the two input signals is 10 V. Besides, the measurement distances from the PZT actuator to a PZT sensor are chosen to be 80 mm, 160 mm, 240 mm, 320 mm and 410 mm, respectively. For the measurement distance of 410 mm case, the PZT sensor is installed on the opposite side of the PZT actuator and on the outer surface of the steel tube of RCFST members.

4.1 Response of PZT sensors at different measurement distances of CHFEMs with randomly distributed aggregates of different shapes under sinusoidal excitation

Figs. 5-6 show the time-domain response of the PZT sensors at different measurement distances from the PZT actuator of the six healthy CHFEMs with randomly distributed elliptical and polygonal aggregates, respectively, under a sinusoidal excitation signal.

From Figs. 5-6, the responses of the PZT sensors of each healthy CHFEM attenuate with the increase of the measurement distance. The response time delay of PZT sensors at different measurement distances can also be seen in Figs. 5-6. Moreover, the response of each PZT sensor at

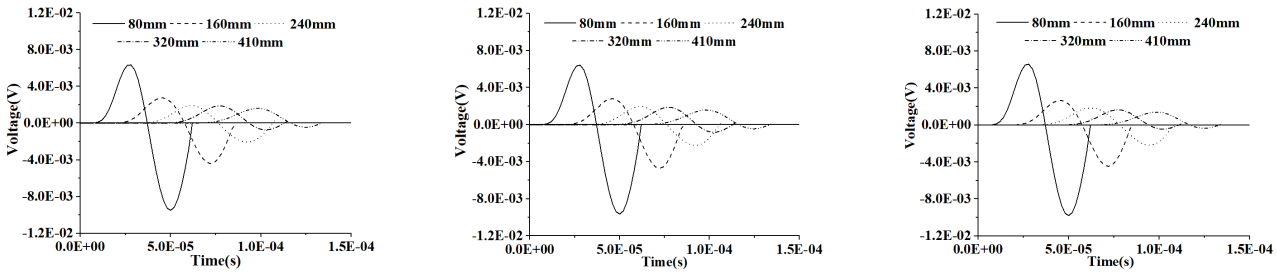

(a) CHFEM E1 (b) CHFEM E2 (c) CHFEM E3

Fig. 5 Time domain responses of PZT sensors at different measurement distances of healthy CHFEMs with randomly distributed elliptical aggregates

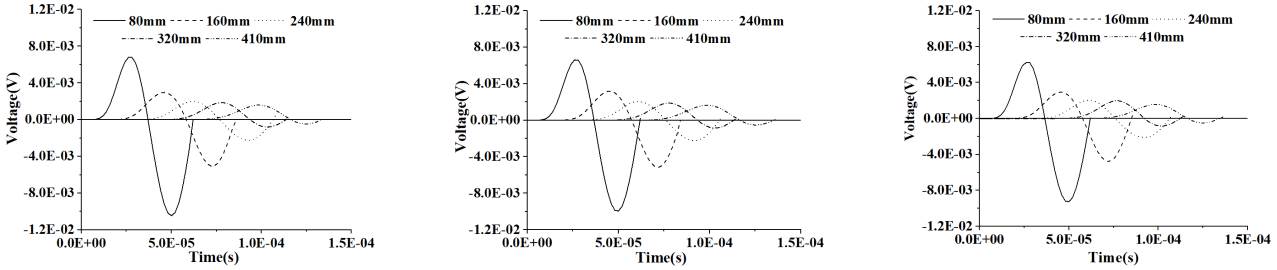

(a) CHFEM P1 (b) CHFEM P2 (c) CHFEM P3

Fig. 6 Time domain responses of PZT sensors at different measurement distances of healthy CHFEMs with randomly distributed polygonal aggregates

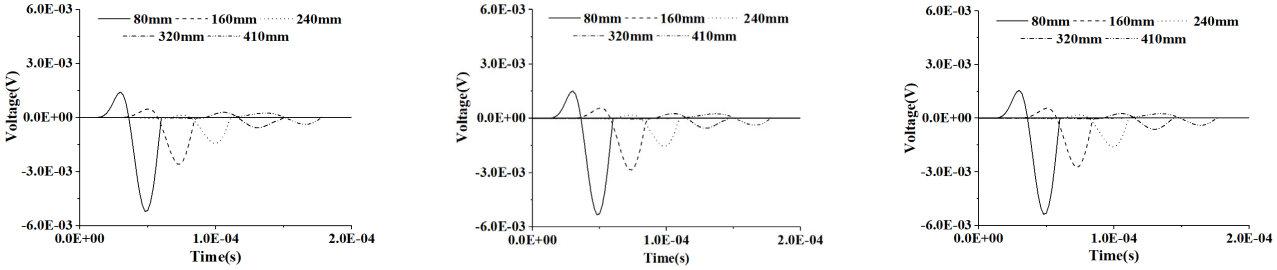

(a) CHFEM E1D (b) CHFEM E2D (c) CHFEM E3D

Fig. 7 Time-domain responses of PZT sensors at different distances of CHFEMs with randomly distributed elliptical aggregates and considering an interface debond defect

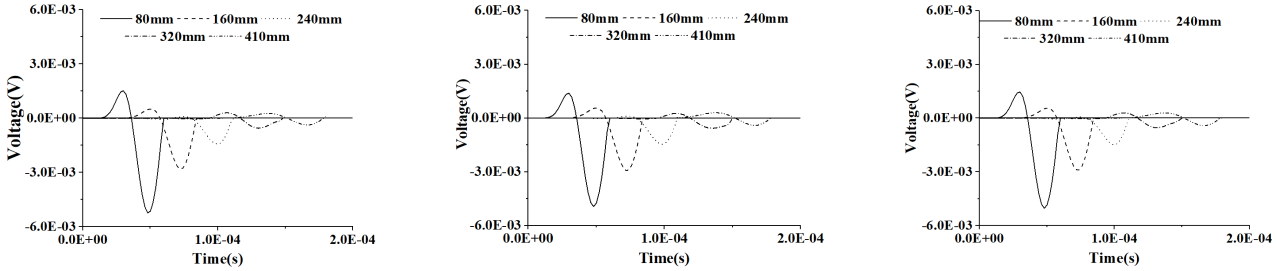

(a) CHFEM P1D (b) CHFEM P2D (c) CHFEM P3D

Fig. 8 Time domain responses of PZT sensors at different distances of CHFEMs with randomly dist-ributed polygonal aggregates and considering an interface debond defect

an identical measurement distance between different CHFEMs with randomly distributed elliptical or polygonal aggregates is very close to each other.

Figs. 7-8 show the time-domain responses of PZT sensors at different distances of the CHFEMs with randomly distributed elliptical and polygonal aggregates

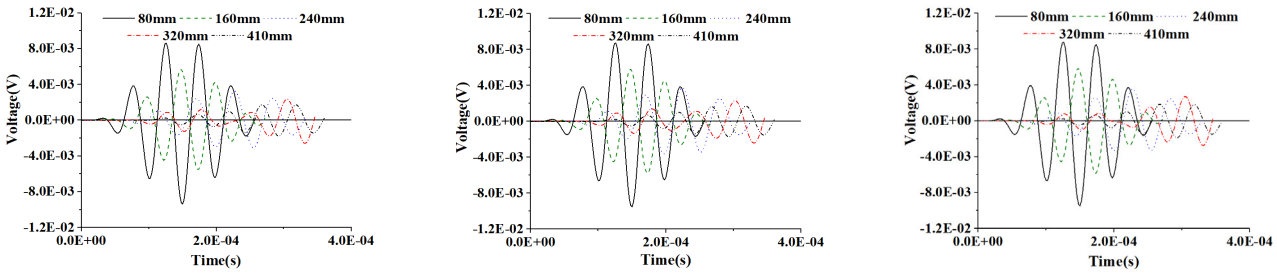

(a) CHFEM E1 (b) CHFEM E2 (c) CHFEM E3

Fig. 9 Time domain responses of PZT sensors at different measurement distances of CHFEMs with random distributed elliptical aggregates

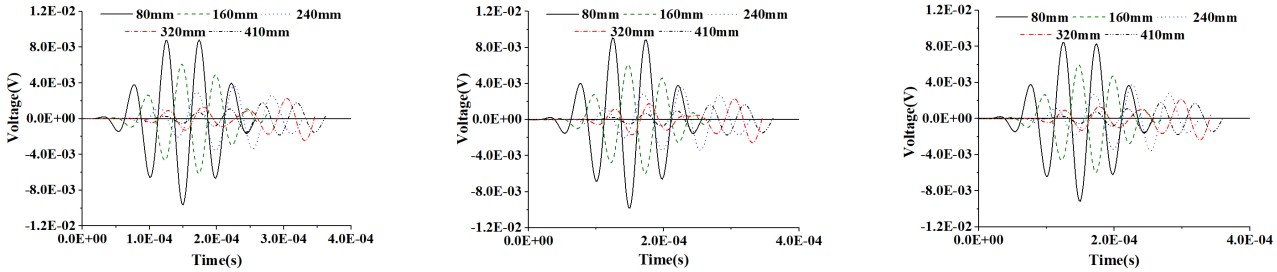

(a) CHFEM P1 (b) CHFEM P2 (c) CHFEM P3

Fig. 10 Time domain responses of CHFEMs with random distributed polygonal aggregates

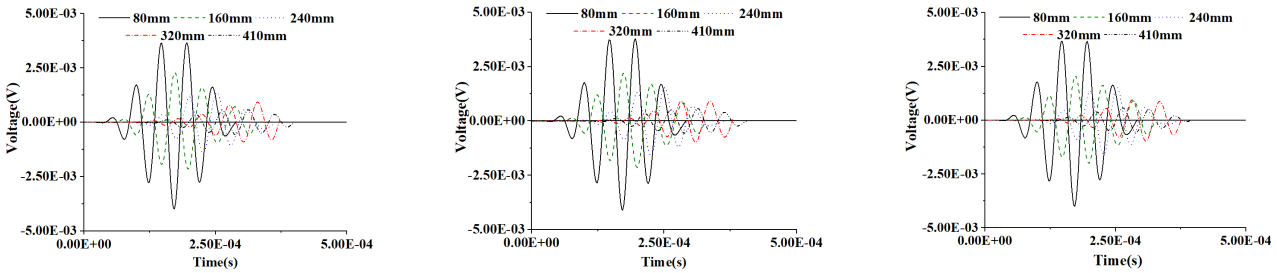

(a) CHFEM E1D (b) CHFEM E2D (c) CHFEM E3D

Fig. 11 Time domain responses of PZT sensors at different distances in CHFEMs with random distributed elliptical aggregates considering an interface debond defect

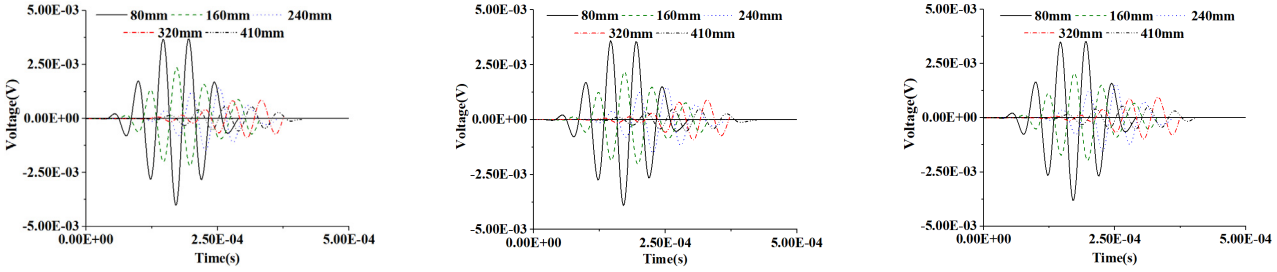

(a) CHFEM P1D (b) CHFEM P2D (c) CHFEM P3D

Fig. 12 Time domain responses of PZT sensors at different distances in CHFEMs with random distri-buted polygonal aggregates considering an interface debond defect

and an identical interface debond defect. The attenuation of stress wave and the response time delay of PZT sensors at different measurement distances can be found in all six CHFEMs with an identical interface debond defect. Comparing the results between the healthy CHFEMs shown in Figs. 5-6 and those with an identical interface debond defect shown in Figs. 7-8, it is clear that the interface debond defect is the dominant factor that affects the

responses of PZT sensors at different measurement distances from the PZT actuator mounted on the outer surface of CHFEMs greatly where the concrete core of the CHFEMs are composed of randomly distributed aggregates with different shapes.

In the following section, the time-domain responses of PZT sensors at different measurement distances of the six healthy CHFEMs and the six CHFEMs with identical interface debond defect under modulated input signal are investigated.

4.2 Responses of PZT sensors at different measurement distances of CHFEMs with randomly distributed aggregates of different shapes under modulated excitation

The time-domain responses of PZT sensors at different measurement distances of the six healthy CHFEMs and the six CHFEMs with identical interface debond defect under modulated input signal are shown in Figs. 9-12.

From Figs. 9-12, the stress wave attenuation and the response time delay between different PZT sensors of all six healthy CHFEMs with randomly distributed elliptical and polygonal aggregates can be observed. Similar findings on the PZT sensor responses at an identical measurement distance of the six CHFEMs without interface debond defect can be found. The similarity of the PZT sensor response at identical measurement distances of the six CHFEMs with an identical interface debond defect also exists. Comparing the response of sensors of the healthy CHFEMs with those of the CHFEMs with an interface debond defect, it is clear to see that the effect of debond defect on the response of each PZT sensor is always dominant.

In the following section, a further quantitative comparison on the influence of different mesoscale concrete cores and interface debond defect on the responses of PZT sensors at different measurement distances of the above six CHFEMs under both sinusoidal and modulated excitation is made to illustrate the difference in the influence of the heterogeneity of concrete core on the response of PZT sensors at different measurement distances.

5. Quantitative comparison on the influence of the heterogeneity and randomness of mesoscale concrete core on the response of PZT sensors at different measurement distances under different excitations

Under sinusoidal excitation, the maximum amplitude of the response of PZT sensors at different measurement distances of the six CHFEMs E1-E3 and P1-P3 studied in this paper are compared with that of the corresponding RCFST members with an interface debond defect and the results are shown in Fig. 13. The simulation results of additional three CHFEMs C1-C3 with circular aggregates investigated in the previous study (Wang *et al*. 2023) are also compared. The nine corresponding CHFEMs with an interface debond defect are named CHFEMs C1D-C3D, E1D-E3D and P1D-P3D, respectively.

From Fig. 13, the heterogeneity of mesoscale concrete core and the shape diversity of the randomly distributed aggregates lead to a relatively large difference in the responses of the PZT sensor with a measurement distance of 80 mm. This means that the measurement of PZT sensor near the actuator is obviously affected by the heterogeneity of mesoscale concrete core and the shape diversity of randomly distributed aggregates in CHFEMs. When the measurement distance from the PZT sensor to the PZT actuator is larger than 160 mm, the difference in the response of PZT sensors between different CHFEMs either with or without an interface debond defect becomes smaller. This indicates that the influence of the heterogeneity of the mesoscale concrete core and the shape diversity of randomly distributed aggregates on the measurement of the PZT sensors is negligible when the measurement distance is over a certain value.

Fig. 14 compares the average value and variance of the maximum amplitude measured by PZT sensors for CHFEM C1-C3, E1-E3, P1-P3 without an interface debond defect and that of the corresponding CHFEMs C1D-C3D, E1D-E3D and P1D-P3D with an interface debonding defect. From Figs. 13 and 14, the interface debond defect causes a significant decline in the maximum amplitude of the response of each PZT sensor of CHFEMs regardless of the distributions and shapes of the aggregates. From Fig. 14(b),

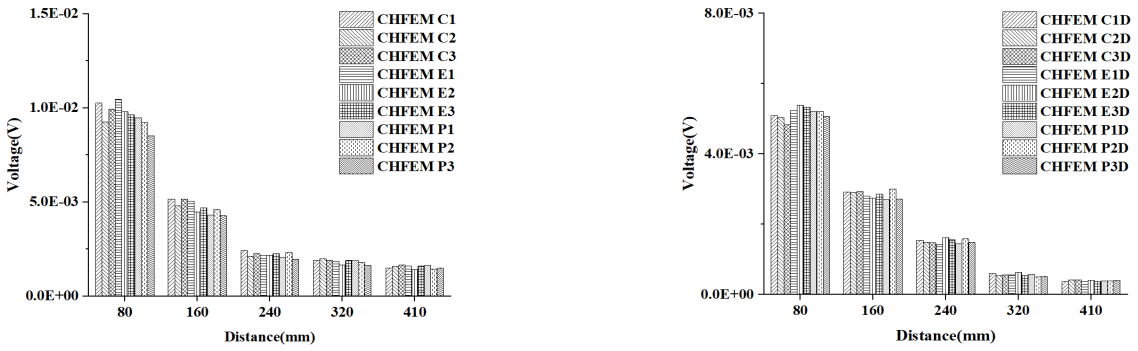

(a) CHFEMs (b) CHFEMs with an interface debond defect

Fig. 13 Comparison of maximum amplitudes of sinusoidal output time domain signals measured by PZT sensors between CHFEMs with different distributions and shapes of aggregate

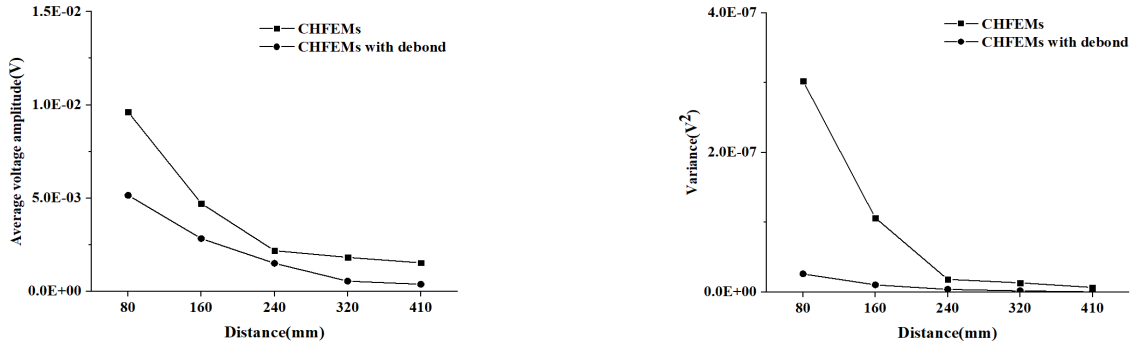

(a) Average voltage amplitude (b) Variance

Fig. 14 The comparison of average amplitude and variance of the responses of PZT sensors shown in Fig. 12 for the CHFEMs with and without an interface debond defect

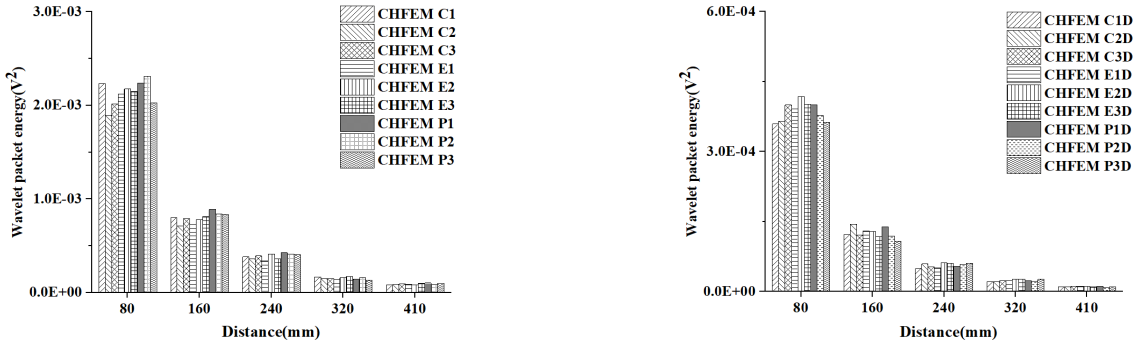

(a) CHFEMs (b) CHFEMs with an interface debond defect

Fig. 15 Quantitative comparison on the wavelet packet energy of PZT sensor between CHFEMs with different aggregates distribution and shapes under modulated excitation

it is found that the variance of the maximum amplitude measured by the PZT sensor close to the PZT actuator of the CHFEMs without an interface debond is the largest. Instead the variation of the maximum amplitudes measured by the PZT sensors at an identical measurement distance of the nine CHFEMs with an interface debond defect is much lower than that of the nine CHFEMs without an interface debond defect. This implies that, for RCFSTs with an interface debond defecct, the influence of the heterogeneity of mesoscale concrete core and the shape diversity of the randomly distributed aggregates on the measurement of PZT sensors is limited when compared with that of interface debond defect.

To explore the attenuation of output signals collected by PZT sensors at different measurement distances in the nine CHFEMs and the corresponding CHFEMs with an identical interface debonding defect under modulated excitation, a more detailed analysis on the wavelet packet energy values of the responses of PZT sensors is performed and the results are shown in Fig. 15.

When the measurement distance from the PZT actuator to the PZT sensor is 80 mm, difference between the wavelet packet energy values of the responses of the PZT sensors in the nine healthy CHFEMs can be observed as shown in Fig. 15. The average and variance of the wavelet packet energy values of each sensor measurement at an identical measurement distance is displayed in Figs. 16(a) and (b). As shown in Fig. 16(a), due to the existence of the interface debond defect in RCFSTs, the wavelet packet energy of PZT sensors decreases obviously regardless of what the measurement distance is. As shown in Fig. 16(b), the influence of the random distribution of aggregates and aggregate shape in concrete core of CHFEMs on the wavelet packet energy values becomes limited with the increase of the measurement distance from the PZT actuator, which is consistent with the results of the CHFEMs with and without the identical interface debond under sinusoidal excitation described above. Moreover, the variance of the wavelet packet energy values of the measurements of the PZT sensors of the nine CHFEMs with an interface debond defect is much smaller than that of the nine CHFEMs without interface debond defect. The dominant influence of the interface debond defect on the response of each PZT sensor of CHFEMs is clear when compared with the random distribution of aggregates of different shapes. This finding is meaningful for interface debond defect detection for RCFSTs using stress wave measurement where concrete core in RCFSTs is a heterogeneous and random material.

Comparing Figs. 14(b) and 16(b), it can be found that the decrease of the variation of the wavelet packet energy values is much more obvious when modulated excitation is employed. Numerical simulation results show that modulated excitation is preferred for interface debond

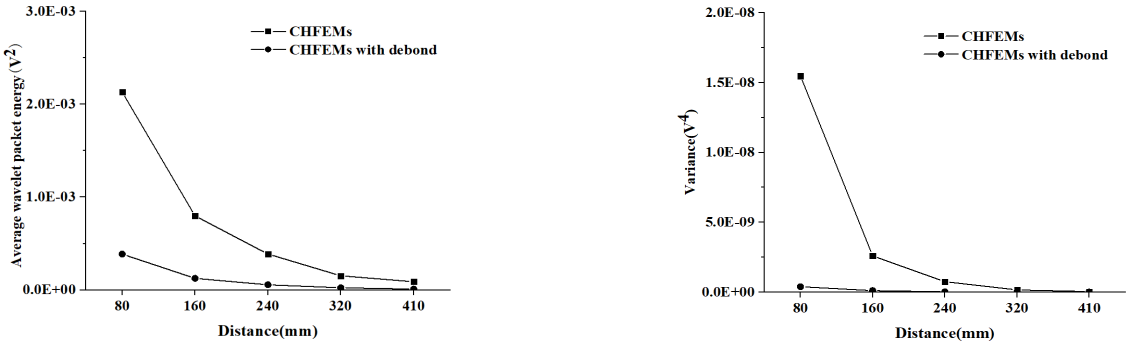

(a) Average wavelet packet energy (b) Variance

Fig. 16 Comparison of average wavelet packet energy and variance of the responses of PZT sensors shown in Fig. 14 for the CHFEMs with and without an interface debond defect

detection in RCFSTs because the influence of the heterogeneity and randomness of the mesoscale structure of concrete core on local sensor measurements with a measurement distance of 240 mm is also limited as shown in Fig. 16(b).

6. Experimental validation on the dominance of interface debond defect on PZT sensor response at different measurement distances

6.1 RCFST specimens and testing setup

To validate the findings from the multi-physics and mesoscale simulations in the previous sections, an experimental study on RCFST cross section specimens considering different measurement distances and an interface debonding defect is performed. Fig. 17 displays a total of thirty plane RCFST cross section specimens. The thirty specimens include fifteen healthy specimens and fifteen specimens with an identical interface debond defect in the middle bottom of each specimen. The debond has a length of 50 mm along the side and a depth of 4 mm. Different PZT sensor measurement distances of 80 mm, 160 mm, 240 mm, 320 mm and 410 mm are considered, respectively. Therefore, for each PZT sensor measurement distance, three groups of healthy RCFST specimens and three groups of specimens with an identical interface debond defect were tested to distinguish the influence of randomness and heterogeneity of the mesoscale concrete core and the interface debond defect on the PZT sensor measurements. The dimension of each experimental specimen is identical to those of the previously mentioned numerical RCFST models.

6.2 Test measurements and analysis

The response of each PZT sensor of each specimen under both sinusoidal and modulated excitation signals are measured as shown in Fig. 18, analyzed and compared to elucidate the effect of interface debond defect on stress wave propagation and PZT sensor measurements in RCFST

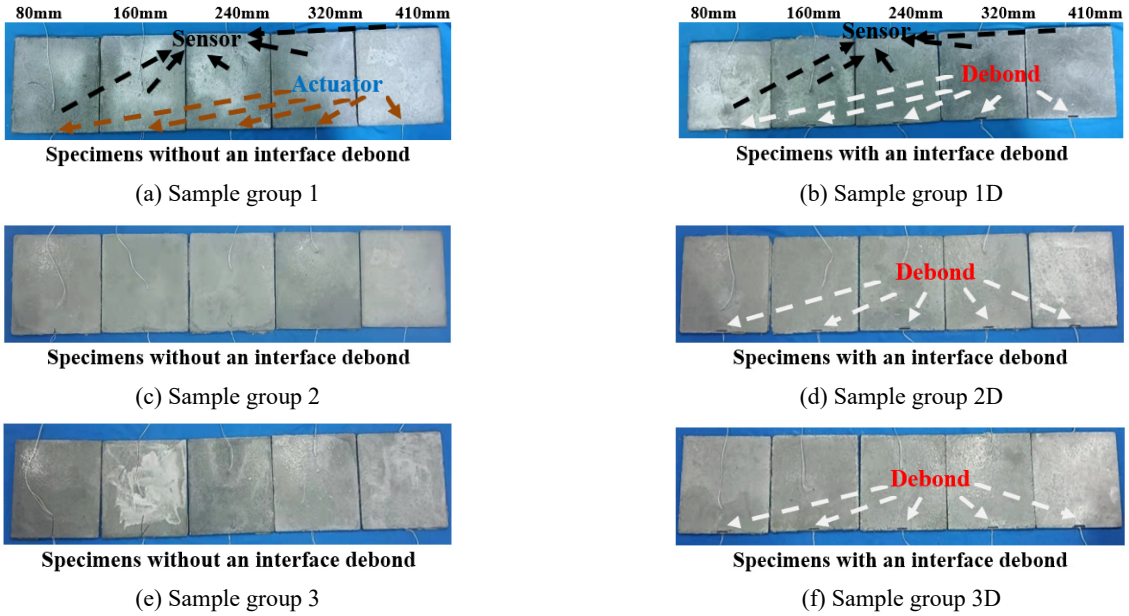

(a) Sample group 1 (b) Sample group 1D

(c) Sample group 2 (d) Sample group 2D

(e) Sample group 3 (f) Sample group 3D

Fig. 17 Specimen group samples

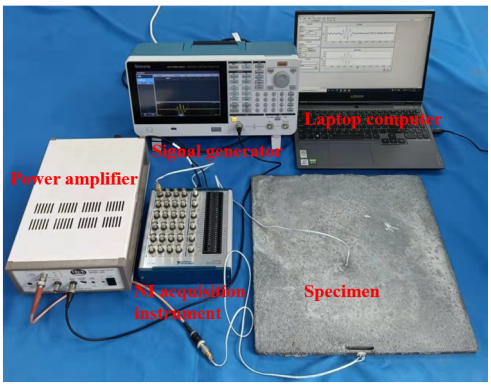

Fig. 18 Testing system for a plane RCFST specimen

members.

6.2.1 Test measurements and analysis on PZT sensor measurements under sinusoidal excitation

Figs. 19 and 20 show the time-domain measurements of the PZT sensors at different measurement distances of the RCFSTs in three sample groups with and without an identical interface debond defect under the sinusoidal excitation signal. The attenuation of stress waves and the response time delay of different PZT sensors can be found. Moreover, comparing the output time-domain signals displayed in Fig. 20 with those displayed in Fig. 19, it is clear to see that the debond defect causes a significant decrease in the measurement of each PZT sensor.

The maximum amplitudes of the PZT sensor measurement of all RCFST specimens with and without the identical debond defect are compared in Fig. 21. From Fig. 21, the difference in mesoscale concrete core of the three RCFST specimen groups results in a certain discrepancy in PZT sensor measurements located closely to the PZT actuator regardless of whether the interface debond exists or not. The average and the corresponding variance of the amplitudes of the PZT sensor measurements at an identical measurement distance are shown in Figs. 22(a) and (b), respectively. As shown in Figs. 21 and 22(a), the amplitude of the measurement of each PZT sensor at each identical measurement distance is smaller than that of healthy RCFST when the interface debond defect exists. Fig. 22(b) shows that the variation of the PZT sensor measurements of the RCFSTs with an interface debond defect is much smaller than that of the RCFSTs without a debond defect. Moreover, the variation of PZT sensor measurements decreases with the increase of the measurement distances, implying that the heterogeneity and randomness of the local mesoscale concrete core of RCFST specimen only affect the responses of PZT sensors locally.

6.2.2 Test measurements and analysis on PZT sensor measurements under modulated excitation

Similarly, the measurements of the PZT sensors of the thirty RCFST specimens under the modulated excitation signal are made and the results are summarized in Figs. 23 and 24. The attenuation of stress wave and the time delay of different PZT sensor measurements with the increase of measurement distance can be observed clearly for RCFSTs either with or without an interface debond defect.

The corresponding wavelet packet energy value of each PZT sensor measurement is displayed in Fig. 25. The average wavelet packet energy values and the corresponding variance of PZT sensor measurements at

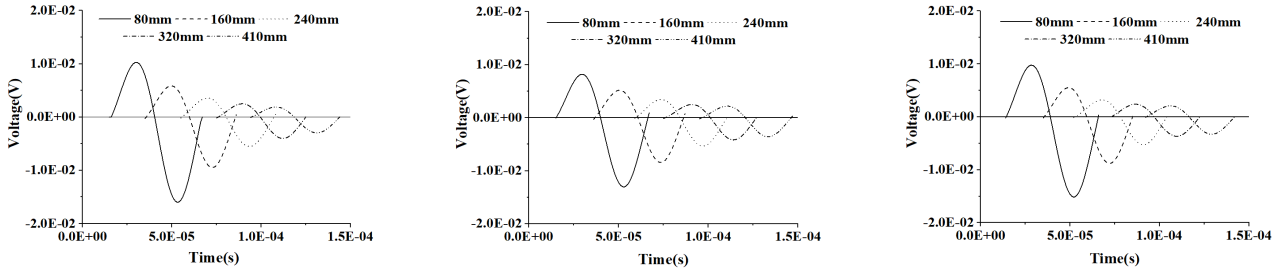

(a) Sample group 1 (b) Sample group 2 (c) Sample group 3

Fig. 19 Time-history of PZT sensors of healthy specimens

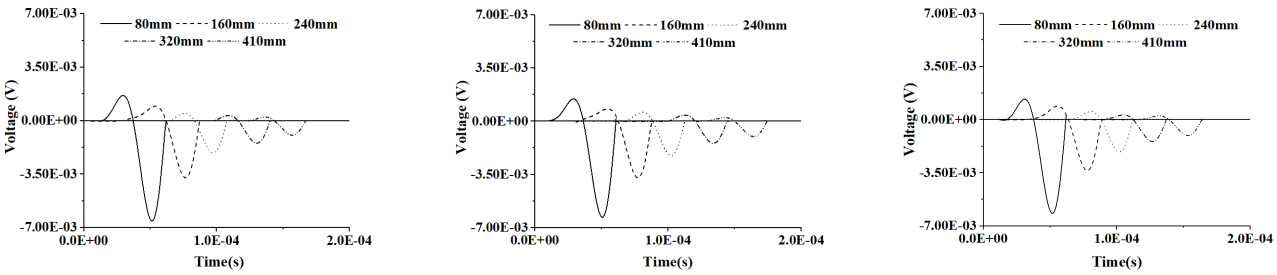

(a) Sample group 1D (b) Sample group 2D (c) Sample group 3D

Fig. 20 Time-history of PZT sensors of specimens with an interface debond defect

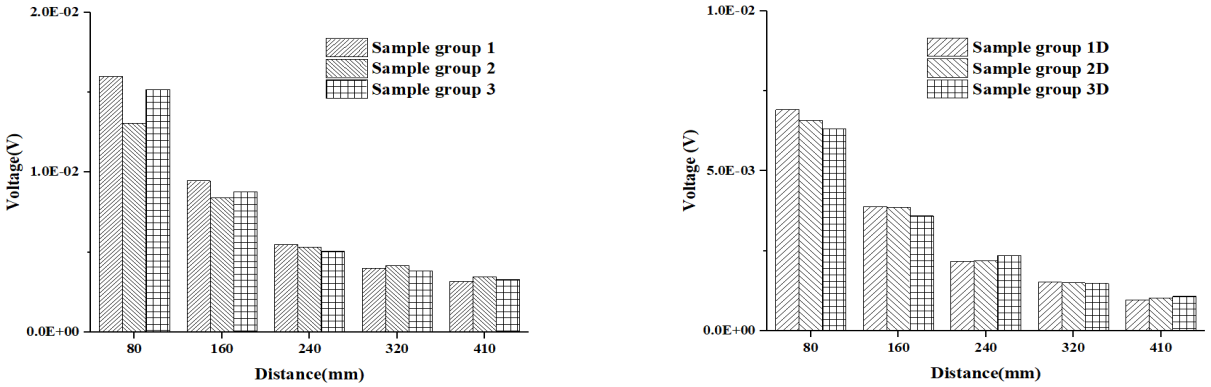

(a) Healthy specimens (b) Debond specimens

Fig. 21 Maximum voltage amplitudes collected by different PZT sensor for RCFST specimens with and without an interface debond defect

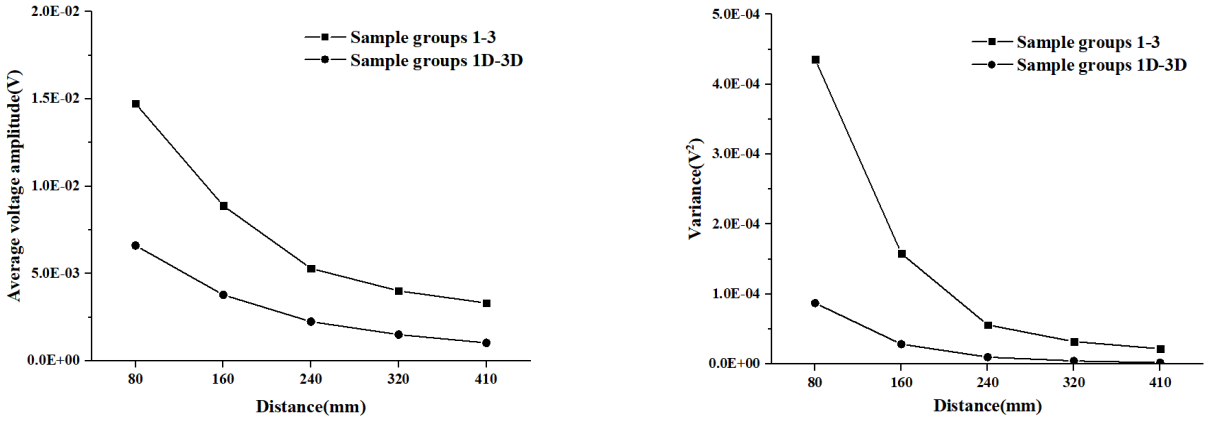

(a) Average voltage amplitude (b) Variance

Fig. 22 Comparison of average amplitude and variance of the responses of PZT sensors shown in Fig. 20 for the sample groups 1-3 with and without an interface debond defect

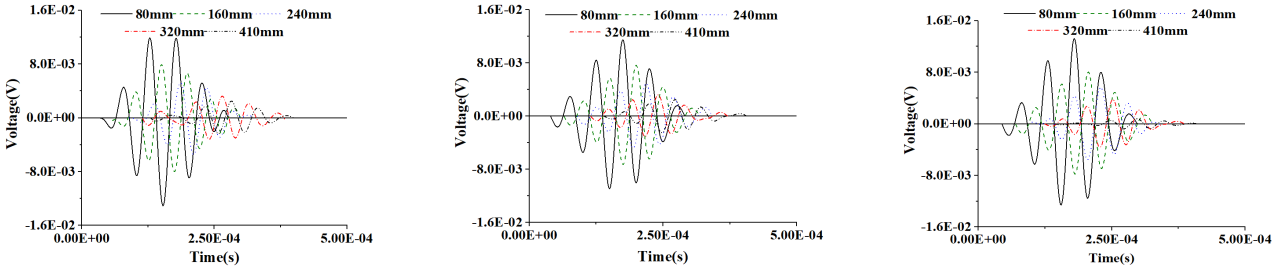

(a) Sample group 1 (b) Sample group 2 (c) Sample group 3

Fig. 23 Time-history of PZT sensor measurements of healthy specimen groups

an identical measurement distance are also shown in Figs. 26(a) and (b). Fig. 25 shows that the inherent heterogeneity and randomness of the local mesoscale concrete core in each RCFST specimen group leads to a certain discrepancy in the wavelet packet energy values of the PZT sensor responses at a measurement distance of 80 mm. When the measured distance of the PZT sensor increases, the difference between the wavelet packet energy values of the measurement of PZT sensors in different RCFST specimens decreases gradually.

From Figs. 25 and 26(a), wavelet packet energy values of PZT sensor measurements of RCFSTs with an interface debond defect are much smaller than those of the RCFSTs without an interface debond defect. From Fig. 26(b), the variance of the wavelet packet energy values of PZT sensors at a certain measurement distance of RCFSTs with an interface debond defect is much smaller than those of the RCFSTs without an interface debond defect. Results show that the effect of the mesoscale structure of concrete as a heterogeneous and random material on the PZT sensor

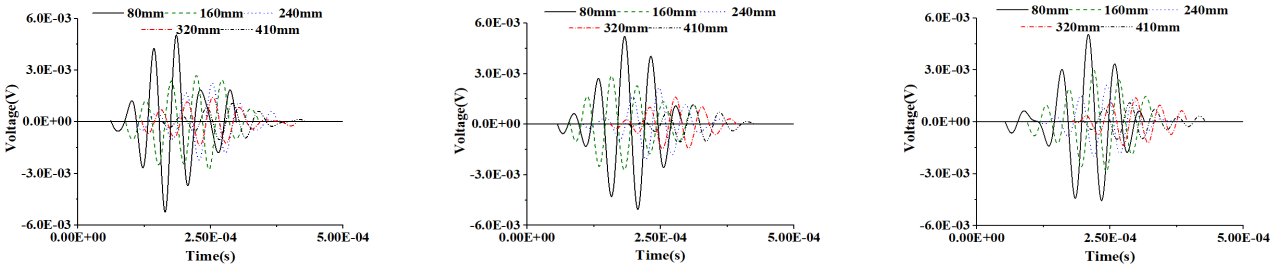

(a) Sample group 1D (b) Sample group 2D (c) Sample group 3D

Fig. 24 Time-history of PZT sensor measurements of specimen groups with an interface debond defect

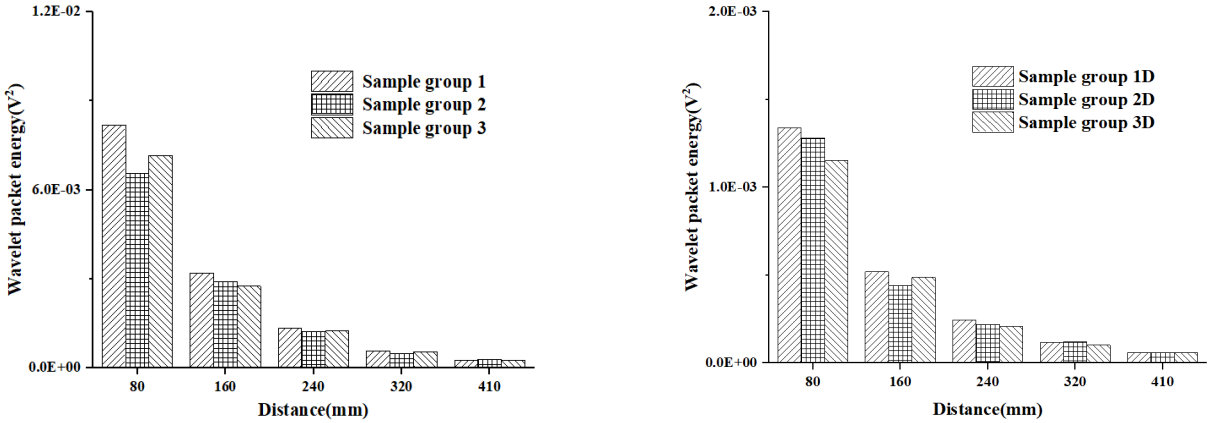

(a) Healthy specimens (b) Debond specimens

Fig. 25 Comparison between wavelet packet energy value of output signals measured by PZT sensor for healthy RCFST specimen groups and those with an interface debond defecT

measurement is very limited, especially for RCFSTs with an interface debond defect.

The experimental results are consistent with those from the multi-physics and mesoscale simulation and validate the feasibility of the interface debond detection method using stress wave measurements from PZT sensors where the concrete core in RCFST members at mesoscale is a typical heterogeneous and random material. The interface debond defect is the dominant factor affecting the PZT sensor measurement and restrains the effect of the heterogeneity and randomness of the mesoscale structure of concrete core on PZT sensor measurement variation.

Comparing Figs. 22(b) and 26(b), it can be found that the decrease in the variation of the wavelet packet energy values is much more obvious when modulated excitation is employed. Experimental results also show that modulated excitation is preferable for interface debond defect detection for RCFSTs since the influence of the heterogeneity and

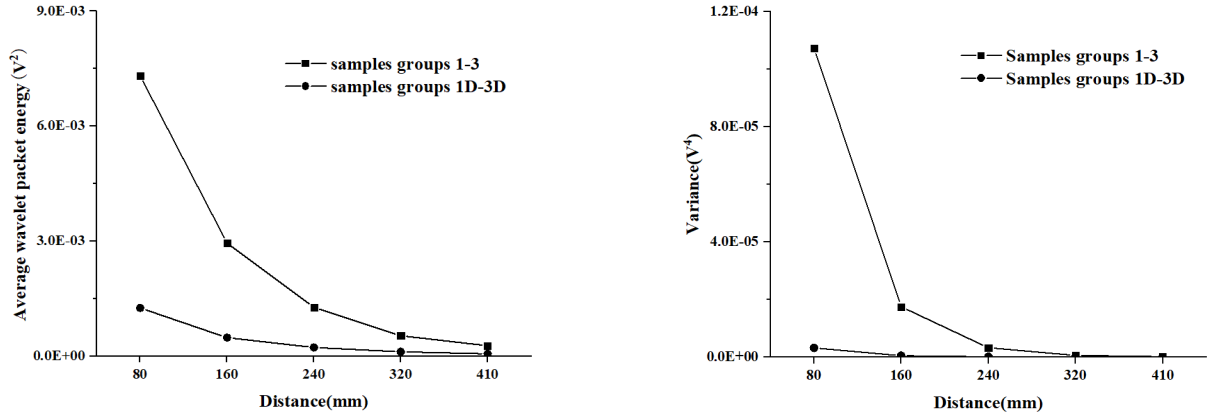

(a) Average wavelet packet energy (b) Variance

Fig. 26 Comparison of average wavelet packet energy values and variance of the responses of PZT sensors shown in Fig. 24 for the sample groups 1-3 with and without debond

randomness of the mesoscale structure of concrete core on local sensor measurements with a measurement distance of 240 mm can also be neglected when interface debond defect exists under a modulated excitation.

7. Conclusions

In this paper, multi-physics and multi-scale CHFEMs are established to distinguish the influence of the heterogeneity and randomness of mesoscale concrete core in RCFSTs with randomly distributed circular, elliptical and polygonal aggregates and that of the interface debond defect on both stress wave fields and the response of PZT sensors at different measurement distances apart from the actuator. To validate the findings from the numerical studies in this paper, experimental validation on thirty RCFST specimens including healthy specimens and those with an identical interface debond defect is carried out and the responses of PZT sensors at different measurement distances are analyzed in detail. The following conclusions can be made according to the numerical simulation and test results.

- The stress wave fields of healthy CHFEMs with randomly distributed circular, elliptical and polygonal aggregates at identical time instants are close to each other. This finding also works for the CHFEMs with an identical interface debond defect, indicating that the influence of the mesoscale heterogeneity and randomness of concrete core on the stress wave fields is very limited. Instead, the debond defect has a significant effect on the stress wave fields of RCFSTs.
- The time-domain output signals and its wavelet packet energy values of the response of PZT sensors at different measurement distances from the PZT actuator of CHFEMs with and without an interface debond defect under different excitation signals show that the heterogeneity and randomness of the mesoscale concrete core locally affect the responses of PZT sensors that are located close to the PZT actuators at a certain degree. For PZT sensors located at a relatively larger measurement distance, the influence of the heterogeneity and randomness of the mesoscale concrete core on PZT sensor measurements is negligible. However, the influence of the interface debond defect on all PZT sensor measurements with different distances is dominant.
- Experimental results on thirty healthy RCFST specimens and specimens with an identical debond defect verify that the response measured by PZT sensors at different measurement distances under both sinusoidal and modulated excitation signals is influenced by the interface debond defect dominantly. The heterogeneity and randomness of mesoscale concrete core on the PZT sensor measurements are very limited, especially for the tested specimens with an interface debond defect.
- Both numerical simulation and experimental results show that modulated excitation is preferred for interface debond defect detection for RCFSTs in practice because the decrease of the wavelet packet energy value variation is much more obvious when modulated excitation is employed.
- The multi-physics and mesoscale numerical simulation and experimental study on stress wave fields and the responses of PZT sensors at different measurement distances for RCFST members with randomly distributed aggregates of different shapes illustrate that the interface debond defect is the major factor leading to variation in stress wave fields and the responses of PZT sensors even concrete core in RCFST members is a typical heterogeneous and random material. The findings from this study validate the rationality of the interface debond detection method for RCFST members using stress wave measurement from PZT sensors.

Acknowledgments

The authors gratefully acknowledge the supports provided by the National Natural Science Foundation of China (Nos. 52378301, 51878305) and the Scientific Research Funds of Huaqiao University (605-50Y18016) to the second author. Partical financial support provided by the U.S. Department of Transportation (USDOT), Office of Assistant Secretary for Research and Technology under the auspices of INSPIRE University Transportation Center at Missouri University of Science and Technology (Grant No. 69A3551747126) is also appreciated. The views, opinions, findings, and conclusions reflected in this publication are solely those of the authors and do not represent the official policy or position of the USDOT or any State or other entity.

References

Abbas, M., Bary, B. and Jason, L. (2023), "3D mesoscale analysis of the effects of steel bar ribs geometry on reinforced concrete bond strength", *Finite Elem. Anal. Des.*, **219**, 103928. https://doi.org/10.1016/j.finel.2023.103928

Abbès, F., Abbès, B., Benkabou, R. and Asroun, A. (2020), "A FEM multiscale homogenization procedure using nanoindentation for high performance concrete", *J. Appl. Comput. Mech.*, **6**(3), 493-504. https://doi.org/10.22055/JACM.2019.29832.1640

Arkadiusz, D., Mieczysław, K., Krzysztof, K. and Tomasz, S. (2021), "Influence of boundary conditions on numerical homogenization of high performance concrete", *Materials*, **14**(4), 1009. https://doi.org/10.3390/ma14041009

Baxter, S.C., Acton, K.A. and Lederle, R.E. (2020), "Determination of representative volume elements for pervious concrete", *Aci. Mater. J.*, **117**(6), 55-63. https://doi.org/10.14359/51728124

Beena, K., Shruti, S., Sandeep, S. and Naveen, K. (2017), "Monitoring degradation in concrete filled steel tubular section using guided waves", *Smart Struct. Syst., Int. J.*, **19**(4), 371-382. https://doi.org/10.12989/sss.2017.19.4.371

Chen, J.Y., Zhang, W.P. and Gu, X.L. (2018), "Mesoscale model for cracking of concrete cover induced by reinforcement corrosion", *Comput. Concrete, Int. J.*, **22**(1), 53-62. https://doi.org/10.12989/cac.2018.22.1.053

Chen, H.B., Xu, B., Wang, J., Luan, L.L. and Mo, Y.L. (2019),

"Interfacial debond detection for rectangular CFST using the MASW method and its physical mechanism analysis at the meso level", *Sensors*, **19**(12), 2778. https://doi.org/10.3390/s19122778

Chen, H.B., Nie, X., Gan, S.Y., Zhao, Y.D. and Qiu, H.H. (2021), "Interfacial imperfection detection for steel-concrete composite structures using NDT techniques: A state-of-the-art review", *Eng. Struct.*, **245**, 123832. https://doi.org/10.1016/j.engstruct.2021.112778

Cai, H. and Deng, F.Q. (2023), "Numerical simulation on the cyclic behavior of ultra-high performance concrete filled steel tubular column", *Struct. Eng. Mech., Int. J.*, **85**(5), 693-707. https://doi.org/10.12989/sem.2023.85.5.693

Dong, Y.J., Su, C. and Qiao, P.Z. (2021), "An improved mesoscale damage model for quasi-brittle fracture analysis of concrete with ordinary state-based peridynamics", *Theor. Appl. Fract. Mech.*, **112**, 102829. https://doi.org/10.1016/j.tafmec.2020.102829

Elias, J. and Cusatis, G. (2022), "Homogenization of discrete mesoscale model of concrete for coupled mass transport and mechanics by asymptotic expansion", *J. Mech. Phys. Solids.*, **167**, 105010, https://doi.org/10.1016/j.jmps.2022.105010

Feng, Q., Kong, Q.Z., Tan, J. and Song, G.B. (2017), "Grouting compactness monitoring of concrete-filled steel tube arch bridge model using piezoceramic-based transducers", *Smart Struct. Syst., Int. J.*, **20**(2), 175-180. https://doi.org/10.12989/sss.2017.20.2.175

Fu, Z.Q., Ji, B.H., Wu, D.Y. and Yu, Z.P. (2019), "Behaviour of lightweight aggregate concrete-filled steel tube under horizontal cyclic load", *Steel Compos. Struct., Int. J.*, **32**(6), 717-729. https://doi.org/10.12989/scs.2019.32.6.717

Geng, X., Moayedi, H., Pan, F.F. and Foong, L.K. (2022), "Predicting the concrete compressive strength through MLP network hybridized with three evolutionary algorithms", *Smart Struct. Syst., Int. J.*, **28**(5), 711-725. https://doi.org/10.12989/sss.2021.28.5.711

Gu, C.P., Ye, G., Wang, Q.N. and Sun, W. (2019), "Modeling of the chloride diffusivity of ultra-high performance concrete with a multi-scale scheme", *Model. Simul. Mater. Sci. Eng.*, **27**(5), 055002. https://doi.org/10.1088/1361-651x/ab1838

Gwon, S.C., Kim, S. and Chang, C.W. (2020), "Prediction of compressive strength of circular CFT confined with braided GFRP tube", *J. Korea Concrete Inst.*, **32**(2), 117-125. https://doi.org/10.4334/JKCI.2020.32.2.117

Hu, P., Moradi, Z., Ali, H.E. and Foong, L.K. (2022), "Metaheuristic-reinforced neural network for predicting the compressive strength of concrete", *Smart Struct. Syst., Int. J.*, **30**(2), 195-207. https://doi.org/10.12989/sss.2022.30.2.195

Jin, L. (2014), *Study on Meso-scopic Model and Analysis Method of Concrete*, Beijing University of Technology, China.

Jin, L., Wang, Z.S.Y., Zhu, H.J., Li, D. and Du, X.L. (2023), "Meso-scale modeling of size effect on pure torsional failure of concrete-filled steel tubular columns", *Struct. Concrete*, **24**(2), 3039-3054. https://doi.org/10.1002/suco.202200678

Li, D.S., Du, F.Z., Chen, Z. and Wang, Y.L. (2016), "Identification of failure mechanisms for CFRP-confined circular concrete-filled steel tubular columns through acoustic emission signals", *Proceedings of the 7th International Conference on Structural Health Monitoring of Intelligent Infrastructure* (*SHMII*), Torino, Italy, July.

Liao, F.Y., Zhang, W.J. and Han, H. (2019), "Cyclic performance of circular concrete-filled steel tubular members with initial gap between tube and concrete core", *Adv. Struct. Eng.*, **23**(1), 174-189. https://doi.org/10.1177/1369433219866291

Liu, J., Liu, Y.J., Zhang, C.Y., Zhao, Q.H., Lyu, Y. and Jiang, L. (2020), "Temperature action and effect of concrete-filled steel tubular bridges: A review", J. Traffic Transp. Eng., 7(2), 174-191. https://doi.org/10.1016/j.jtte.2020.03.001.

Liu, Q., Xu, B., Chen, G., Ni, W., Liu, Z., Lin, C. and Zhuang, Z. (2024a), "Experimental study on the detection of the existence and location of mimicked and unexpected interface debonding defects in an existing rectangular CFST column with PZT Materials", *Materials*, **17**(13), 3154. https://doi.org/10.3390/ma17133154

Liu, Q., Xu, B., Xia, Z., Chen, Z., Yao, Y. and Wang, J. (2024b), "Interface debonding defect detection for CFST columns based on EMI measurements: experiment, numerical simulation and blind inspection in practice", *Adv. Struct. Eng.*, **27**(7), 1151-1169, https://doi.org/10.1177/13694332241242297

Luan, L., Xu, B., Chen, H. and Wang, H. (2021), "Local wave propagation analysis in concrete-filled steel tubes with spectral element method using absorbing layers – Part II: Application in coupling system", *Mech. Syst. Signal Process.*, **146**, 107004. https://doi.org/10.1016/j.ymssp.2020.107004

Mei, Q.Q., Wu, Z.Y., Yu, H.F., Zhang, J.H. and Ma, H.Y. (2023), "Multiscale analysis on the mechanical behavior and failure mechanism of high strength concrete", *Struct. Concrete*, **24**(5), 6467-6484. https://doi.org/10.1002/suco.202200215

Rezakhani, R., Zhou, X. and Cusatis, G. (2017), "Adaptive multiscale homogenization of the lattice discrete particle model for the analysis of damage and fracture in concrete", *Int. J. Solids Struct.*, **125**, 50-67. https://doi.org/10.1016/j.ijsolstr.2017.07.016

Shen, M.Y., Shi, Z., Zhao, C., Zhong, X.G., Liu, B. and Shu, X.J. (2019), "2-D meso-scale complex fracture modeling of concrete with embedded cohesive elements", *Comput. Concrete*, *Int. J.*, **24**(3), 207-222. https://doi.org/10.12989/cac.2019.24.3.207

Song, G., Chen, D. and Huo, L. (2019), "Interface debonding detection of concrete filled steel tubular (CFST) based on the acoustic signal", *Proceedings of the 9th International Conference on Structural Health Monitoring of Intelligent Infrastructure*: *Transferring Research into Practice*, St. Louis, MO, USA, August.

Wang, J., Xu, B., Chen, H.B., Ge, H.B. and Zhou, T.M. (2022a), "Multi-physics mesoscale substructure analysis on stress wave measurement within CFST-PZT coupling models for interface debond detection", *Sensors*, **22**(3), 1039. https://doi.org/10.3390/s22031039

Wang, J., Xu, B., Chen, H.B., Ge, H.B. and Wang, C. (2022b), "Mesoscale numerical analysis and test on the effect of debond defect of rectangular CFSTs on wave propagation with a homogenization method", *Mech. Syst. Signal Proc.*, **163**, 108135. https://doi.org/10.1016/j.ymssp.2021.108135

Wang, B., Zhu, E.Y. and Zhang, Z. (2022c), "Microscale fracture damage analysis of lightweight aggregate concrete under tension and compression based on cohesive zone model", *J. Eng. Mech.*, **148**(2), 04021153. https://doi.org/10.1061/(ASCE)EM.1943-7889.0002051

Wang, J., Xu, B., Liu, Q., Guan, R.Q. and Ma, X.G. (2023), "Feasibility of stress wave-based debond defect detection for RCFSTs considering the influence of randomly distributed circular aggregates with mesoscale homogenization methodology", *Materials*, **16**, 3120. https://doi.org/10.3390/ma16083120

Xu, B., Li, B. and Song, G.B. (2013a), "Active debond detection for large rectangular CFSTs based on wavelet packet energy spectrum with piezoceramics", *J. Struct. Eng.*, **139**(9), 1435-1443. https://doi.org/10.1061/(ASCE)ST.1943-541X.0000632

Xu, B., Zhang, T., Song, G.B. and Gu, H. (2013b), "Active interface debond detection of a concrete-filled steel tube with piezoelectric technologies using wavelet packet analysis", *Mech. Syst. Signal Proc.*, **36**(1), 7-17. https://doi.org/10.1016/j.ymssp.2011.07.029

Xu, B., Chen, H.B. and Xia, S. (2017a), "Numerical study on the

mechanism of active interfacial debonding detection for rectangular CFSTs based on wavelet packet analysis with piezoceramics", *Mech. Syst. Signal Proc.*, **86**, 108-121. https://doi.org/10.1016/j.ymssp.2016.10.002

Xu, B., Chen, H.B. and Xia, S. (2017b), "Wave propagation simulation and its wavelet package analysis for debond detection of circular CFST members", *Smart. Struct. Syst.*, *Int. J.*, **19**(2), 181-194. https://doi.org/10.12989/sss.2017.19.2.181

Xu, B., Chen, H.B., Mo, Y.L. and Chen, X. (2017c), "Multi-physical field guided wave simulation for circular concrete-filled steel tubes coupled with piezoelectric patches considering debond defects", *Int. J. Solids Struct.*, **122**, 25-32. https://doi.org/10.1016/j.ijsolstr.2017.05.040

Xu, B., Chen, H.B., Mo, Y.L. and Zhou, T.M. (2018), "Dominance of debond defect of CFST on PZT sensor response considering the meso-scale structure of concrete with multi-scale simulation", *Mech. Syst. Signal Proc.*, **107**, 515-528. https://doi.org/10.1016/j.ymssp.2018.01.041

Xu, B., Luan, L., Chen, H., Wang, J. and Zheng, W. (2019), "Experimental study on active interface debonding detection for rectangular concrete-filled steel tubes with surface wave measurement", *Sensors*, **19**(15), 3248. https://doi.org/10.3390/s19153248

Xu, B., Luan, L., Chen, H. and Wang, H. (2020), "Local wave propagation analysis in concrete-filled steel tube with spectral element method using absorbing layers – Part I: Approach and validation", *Mech. Syst. Signal Process.*, **140**, 106644. https://doi.org/10.1016/j.ymssp.2020.106644

Xu, B., Fan, X., Wang, H., Zhou, S., Wang, C., Chen, H. and Ge, H. (2021), "Experimental study on grout defects detection for grouted splice sleeve connectors using stress wave measurement", *Constr. Build. Mater.*, **274**, 121755. https://doi.org/10.1016/j.conbuildmat.2020.121755

Yan, S., Lin, J.Y. and Zhang, B.W. (2018), "Feasibility research on interface debonding detection in concrete filled steel tubular columns using PZT-based guided waves", *Proceedings of the 16th Biennial International Conference on Engineering, Science, Construction, and Operations in Challenging Environments* (*Earth & Space*), Cleveland, OH, USA.